T_0 is a $^3\pi\pi^*$ state. In the wave function of this state π-electron correlation hardly plays a role; T_0 is well represented by a single configuration that corresponds to an excitation of a single electron from the highest occupied π to the lowest unoccupied π^* molecular orbital. In view of such a simple description of T_0 it would be worthwhile to try and calculate from the present ab initio wave function the zero-field splittings of T_0 and the spin-density distribution along the polyenal chain. Finally, for octatrienal we have found a large difference between the calculated radiative lifetime of the T_z sublevel of T_0 and the experimentally observed radiationless lifetime. This discrepancy even increases on lengthening the chain and explains the total absence of polyenal phosphorescence.

Acknowledgment. The Theoretical Chemistry group of the University of Bonn is acknowledged for making available the MRD-CI computer program. We thank J. H. van der Waals for stimulating discussions concerning the treatment of the spin-orbit coupling and Aafke Stehouwer for her contributions to the calculations. This work was supported by The Netherlands Foundation for Chemical Research (SON) with financial aid from The Netherlands Organization for Scientific Research (NWO).

Theoretical Study on Mechanism and Selectivity of Electrophilic Aromatic Nitration

Kálmán J. Szabó,* Anna-Britta Hörnfeldt, and Salo Gronowitz

Contribution from the Division of Organic Chemistry 1, Chemical Center, University of Lund, P. O. Box 124, S-221 00 Lund, Sweden. *Received January 6, 1992*

Abstract: Reaction profiles for the aromatic nitration reaction have been calculated. Stationary points were located and characterized at the ab initio HF/3-21G level. Single point MP4DQ/3-21G calculations were carried out to evaluate the correlation energy correction for the activation barrier heights. Unsolvated nitronium ion reacts with benzene to give the Wheland intermediate without an energy barrier. Solvated nitronium ion (protonated methyl nitrate) reacts with aromatics to give an activation barrier which is substituent dependent, but also depends on the solvating species. The positional selectivity is produced after this barrier and is independent of the matrix effects. Some predictions were made with regard to the condensed phase nitration reaction.

Aromatic nitration is of outstanding importance in the theory of organic reactivity. In spite of the huge body of accumulated data, the mechanism of aromatic nitration continues to be the subject of active research and some controversy.[1,6] An interesting feature is, for example, that the rate of nitration of toluene relative to benzene depends strongly on the solvent and reagent, while the ratio of ortho-, meta-, and para-substituted products only slightly varies (Table I).

The theoretical investigation of aromatic nitration is complicated by the fact that most of the findings refer to condensed-phase experimental conditions, and the role of solvent effects is not clear. Examining the gas-phase reaction of protonated alkyl nitrates with aromatics, Cacace and Attinâ[4,5,7] pointed out the fundamental similarity between gas-phase and liquid-phase nitration. These gas-phase studies opened new perspectives for the theoretical investigation of mechanistic details of the aromatic nitration.

Computational Aspects

The Gaussian 86 and Gaussian 90 computer programs[8] were used on a Cray X/MP-416 supercomputer. Restricted Hartree-Fock (RHF) calculations and fourth-order Møller-Plesset correlation energy calculations for double and quadruple substitutions (MP4DQ) were performed using the split valence 3-21G basis set. Stationary structures and points of reaction profiles were optimized by using Schlegel's gradient technique.[9] The final optimization of the stationary points was carried out with no restrictions on internal coordinates. The optimization of the possible Wheland intermediates (WI) and transition states (TS) of benzene nitration continued until the largest remaining force was less than 0.0001 au. The reason for this rather tight convergence criterion is our interest in the structure of these species. The optimization of TS structures is complicated by the flat potentials of geometry parameters describing the conformation of reagent relative to the ring system. The very slow convergence of the geometry optimization of π-complexes is due to the same problem. Therefore, their geometries were optimized until the forces dropped below 0.002 au, but it was ensured that their total energy did not change more than 0.05 kJ/mol in the last five geometry-optimization steps. At the highest level of theory, MP4DQ/3-21G single point calculations were performed on the HF/3-21G geometries of stationary points obtained along the benzene nitration pathways.

Results and Discussion

Reaction of Benzene with Nitronium Ion. The energy profile for the reaction between benzene and the nitronium ion was calculated (Table II, Figure 1). The distance between the nitrogen atom of the nitronium ion and the attacked carbon atom was chosen as the reaction coordinate (RC). Points of the reaction profile were obtained by freezing the reaction coordinate and optimizing the rest of the internal coordinates simultaneously. No activation barrier was found along the chosen reaction coordinate. The experimental results led to the same conclusions: the gas-phase reaction of benzene with nitronium ion is very exothermic, and vitually no energy barrier is involved.[10] At large RC values

(1) Olah, G. A. *Nitration Methods and Mechanisms*; VCH: New York, 1989; pp 117-218.
(2) Masci, B. *Tetrahedron* **1989**, *45*, 2719.
(3) Masci, B. *J. Chem. Soc., Chem. Commun.* **1982**, 1262.
(4) Attinâ, M.; Cacace, F. *Gazz. Chim. Ital.* **1988**, *118*, 241 and references therein.
(5) Attinâ, M.; Cacace, F.; Ricci, A. *Tetrahedron* **1988**, *44*, 2015.
(6) Schofield, K. *Aromatic Nitration*; Cambridge University Press: Cambridge, 1980; pp 44-54, 104-128.
(7) Attinâ, M.; Cacace, F.; Yañez, M. *J. Am. Chem. Soc.* **1987**, *109*, 5092.
(8) Frisch, M. J.; Head-Gordon, M.; Trucks, G. W.; Foresman, J. B.; Schlegel, H. B.; Raghavachari, K.; Robb, M. A.; Gonzales, C.; Whiteside, R. A.; Seeger, R.; Melius, C. F.; Baker, J.; Binkley, J. S.; DeFrees, D. J.; Fox, D. J.; Martin, R. L.; Khan, L. R.; Stewart, J. J. P.; Topiol, S.; Flender, E. M.; Pople, J. A. *Gaussian 86* and *Gaussian 90*, Gaussian, Inc.: Pittsburgh, PA, 1986 and 1990.
(9) Schlegel, H. P. *J. Comput. Chem.* **1982**, *3*, 214.
(10) Morrison, J. D.; Stanney, K.; Tedder, J. M. *J. Chem. Soc., Perkin Trans. 2* **1981**, 967.

0002-7863/92/1514-6827$03.00/0

Table I. Orientation and Relative Reactivity in the Nitration of Toluene

reagent	solvent or bulk gas	pressure (Torr)	rel rate[a]	orientation (%) o	m	p	ref
HNO_3	H_2SO_4		20	56	5	39	1
HNO_3	AcOH		24	56	4	40	1
HNO_3	CH_3NO_2		21	59	4	37	1
Bu_4NNO_3/TFAA	CH_3NO_2		26	60	4	36	2
Bu_4NNO_3/TFAA	sulfolane		42	63	3	34	2
Bu_4NNO_3/TFAA	CH_2Cl_2		58	57	2	41	2
NO_2BF_4	sulfolane		1.7	65	3	32	1
NO_2BF_4/CE[b]	CH_2Cl_2		77	12	1	87	3
NO_2ClO_4	sulfolane		1.6	66	3	31	1
$MeO^+(H)NO_2$	CH_4	720	7.7	58	6	36	4
$MeO^+(H)NO_2$	CH_4	100	2.9	51	11	38	4
$MeO^+(H)NO_2$	H_2	720	1.5	50	14	36	4
$CF_3CH_2O^+(H)NO_2$	CH_4	760	2.1	52	14	34	5
$(CF_3)_2CHO^+(H)NO_2$	CH_4	760	1.4	46	9	45	5

[a] With respect to rate of nitration of benzene as unity. [b] Crown ether (21-crown-7).

Table II. Energy Profile for the Reaction of Nitronium Ion with Benzene

RC[a] (Å)	E_{total} (au)	ΔE^b (kJ/mol)
∞	−431.879 505	0.0
3.8	−431.895 959	−43.2
3.4	−431.902 070	−59.2
3.2	−431.903 574	−63.2
3.0	−431.905 373	−67.9
2.8	−431.907 009	−72.2
2.4	−431.917 254	−99.1
2.2	−431.925 911	−121.8
1.8	−431.947 717	−179.1
1.5[c]	−431.968 714	−234.2

[a] Reaction coordinate. Distance between the nitrogen atom and the attacked carbon atom. [b] Relative to the separated reactants. [c] Wheland intermediate.

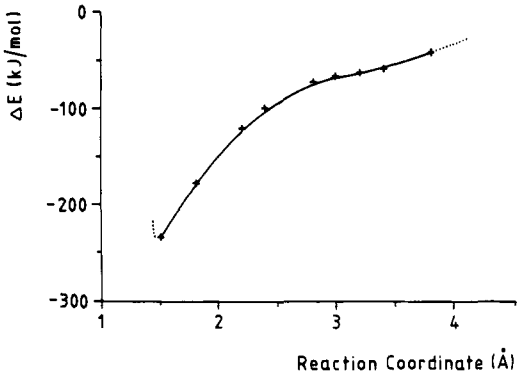

Figure 1. Energy profile for reaction of benzene with nitronium ion.

(3–4 Å), the gradient along this coordinate is diminished, obviously due to the large distance between the reactants. However, a stationary point (π-complex or weakly bound complex) could not be localized on the potential energy surface, since by releasing the reaction coordinate the geometry converged toward the Wheland intermediate. The geometry given by Gleghorn et al.[11] was optimized until the above-mentioned tight convergence criterion was reached. Harmonic vibrational frequencies were calculated at the HF/3-21G level for the resulting geometry. No imaginary frequencies were found, proving that this structure must be a real minimum on the potential energy hypersurface. While the electrostatic repulsion between the positively charged species led to an activation barrier[12,13] for the reaction between dithienopyridinium ion and nitronium ion, only attractive interactions appear between the uncharged electron-rich benzene ring and the

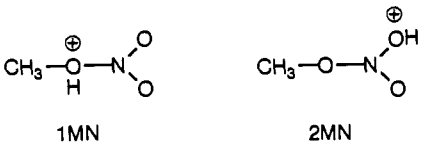

Figure 2. Possible isomers of protonated methyl nitrate (MN).

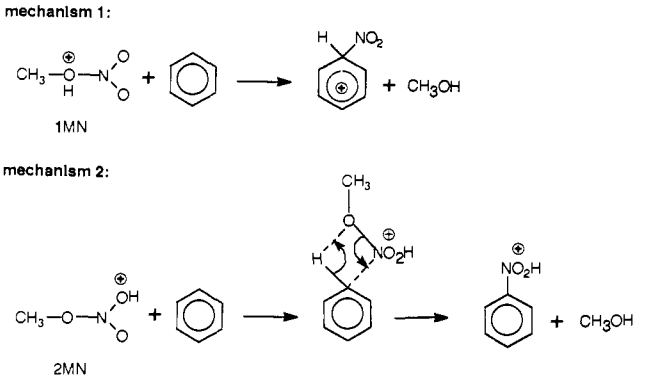

Figure 3. Possible reaction mechanisms for reaction of benzene with protonated methyl nitrate.

positively charged nitronium ion. Notwithstanding, this conclusion raises the question, how can nitration of uncharged aromatics possess high selectivity, if the formation of Wheland intermediates is not accompanied by any activation barrier.

Reaction of Benzene with Protonated Methyl Nitrate. Recently, Dewar et al.[14] called attention to solvent effects in ion–molecule reactions, which lack a transition state in theoretical calculations related to gas-phase conditions, but proceed with measurable activation energy in the condensed phase. Dewar[14] introduced a new term; desolvation barrier (DSB), for entirely solvent-related activation barriers, as distinguished from the intrinsic barriers (IB) due to the chemical processes. Considering the calculated reaction profile (Figure 1) and the exothermic formation of the Wheland intermediate, we also believe that the nitration of benzene derivatives is a DSB-type process.

In order to prove this hypothesis we calculated the structure and stability of Wheland intermediates and transition states occurring in the gas-phase nitration of benzene and toluene by protonated methyl nitrate.[4,7]

Methyl nitrate can be protonated on two different places (Figure 2): on the oxygen atom of the methoxy group (1MN) and on the terminal oxygen atoms (2MN). Therefore Cacace and Attinà[7,15] proposed two alternative mechanisms for the nitration reaction: according to mechanism 1 (Figure 3), 1MN reacts with aromatics

(11) Gleghorn, J. T.; Torossian, G. *J. Chem. Soc., Perkin Trans. 2* **1987**, 1303.
(12) Szabó, K. J.; Hörnfeldt, A.-B. *THEOCHEM*, in press.
(13) Szabó, K. J.; Hörnfeldt, A.-B.; Gronowitz, S. *J. Org. Chem.* **1991**, *56*, 1590.
(14) Dewar, M. S. J.; Storch, D. M. *J. Chem. Soc., Perkin Trans. 2* **1989**, 877.
(15) Bernardi, F.; Cacace, F.; Grandinetti, F. *J. Chem. Soc., Perkin Trans. 2* **1989**, 413.

Table III. Energy Profile for the Reaction of the Protonated Methyl Nitrate with Benzene

RC (Å)	E_{total} (au)	mechanism 1[a] ΔE (kJ/mol)	mechanism 1[a] R_{N-OCH_3}[b] (Å)	E_{total} (au)	mechanism 2[a] ΔE (kJ/mol)	mechanism 2[a] R_{N-OCH_3}[b] (Å)
∞	546.339 326	0.0		−546.362 999	0.0	
4.5	−546.363 814	−64.3	1.621	−546.377 838	−38.9	1.356
3.5	−546.369 057	−78.1	1.535	−546.388 810	−67.7	1.356
3.0	−546.352 863	−35.5	1.632	−546.381 910	−49.7	1.356
2.7	−546.346 868	−19.8	2.160	−546.376 363	−35.1	1.363
2.5	−546.345 737	−16.8	2.273	−546.364 573	−4.1	1.375
2.3	−546.346 022	−17.6	2.404	−546.360 030	7.8	1.376
2.0	−546.354 805	−40.6	2.659	−546.347 865	39.7	1.426
1.8	−546.371 036	−83.2	2.742	−546.356 938	15.9	1.427
1.6	−546.384 514	−118.6	2.757			
1.5	−546.395 456	−147.4	2.593	−546.397 022	−89.3	1.431

[a] See Figure 3. [b] Calculated distance between the nitrogen atom and the oxygen atom of the methoxy group in the corresponding reagent.

Table IV. Energies and Characterization of the Optimized Stationary Points

species[a]	HF/3-21G//HF/3-21G E_{total} (au)	ΔE (kJ/mol)	E_{rel}[b] (kJ/mol)	MP4DQ/3-21G//HF/3-21G E_{total} (au)	ΔE (kJ/mol)	E_{rel}[b] (kJ/mol)	NIF[c]	IF[d] (cm^{-1})	E_{zpv}[e] (kJ/mol)
1MN	−316.919 881			−317.534 218			0		175.8
S1[f]	−546.339 326	0.0		−547.500 152	0.0		0		461.5
1BPA	−546.369 057	−78.1	0.0	−547.529 911	−78.1	0.0	0		465.3
1BPB	−546.349 659	−27.1	51.0	−547.514 523	−37.7	40.4	1	15*i*	464.3
1BTS	−546.345 737	−16.8	61.3	−547.512 443	−32.2	45.8	1	264*i*	463.8
1BWM	−546.395 456	−147.2	−69.1	−547.536 053	−94.3	−16.1			
1BW[g]	−431.968 714						0		316.9
2MN	−316.943 554			−317.541 756			0		179.8
S2[h]	−546.362 999	0.0		−547.507 690	0.0		0		465.5
2BP	−546.388 810	−67.7	0.0	−547.536 366	−75.3	0.0	1	20*i*	466.6
2BTS	−546.347 865	39.7	107.4	−547.503 547	10.9	86.2	1	475*i*	467.0
2BW	−546.397 022	−89.3	−21.6	−547.514 917	−19.0	56.3	0		472.5

[a] See Figure 5 for notation. [b] Energy relative to the corresponding electrostatic complex. [c] Number of imaginary frequencies. [d] Value of the imaginary frequency. [e] Zero-point vibration energies. [f] Separated reactants of mechanism 1. [g] Isolated Wheland intermediate (without methanol solvation). [h] Separated reactants of mechanism 2.

leading to the classical Wheland intermediate; while according to mechanism 2, 2MN reacts with aromatics, including a concerted process, leading directly to O-protonated nitrobenzene. Mass spectrometric measurements[16] gave evidence that both isomers are present under the nitration conditions. Theoretical calculations reported by Bernardi et al.[15] refer to a more stable 2MN isomer in the gas phase. Its calculated stability depends on the basis set used: −152 kJ/mol and −28 kJ/mol on STO-3G and 4-31G levels, respectively, relative to the total energy of the 1MN isomer. Similarly, the 2MN isomer was found to be more stable than 1MN by 67 kJ/mol at the 3-21G level. The two reaction paths (Figure 3) result in products with different stabilities. The O-protonated nitrobenzene (total energy: −432.041 153 au), which should be formed in the concerted reaction 2, is considerably (190 kJ/mol) more stable than the isoelectronic and isodesmic Wheland intermediate. However, the lack of a kinetic isotope effect[7] makes the classical mechanism 1 more probable.

In order to elucidate the ambiguity concerning the mechanism of the gas-phase nitration, reaction profiles were calculated for both alternatives. The definition of the reaction coordinate and the method of calculation were the same as for the benzene–nitronium ion reaction. In contrast to this reaction, both energy profiles show two minima and one maximum (Figure 4, Table III).

Harmonic frequencies were calculated (at the HF/3-21G level) to characterize the stationary points obtained (Table IV). The Wheland intermediate complex 1BW (without methanol) and the covalent complex 2BW (Figure 5) gave only real frequencies. Large imaginary frequencies characterized 1BTS and 2BTS as first-order saddle points. The weakly bound complex 1BPA gave only real frequencies, while 1BPB and 2BP gave small imaginary frequencies. However, it is very likely that these small imaginary frequencies are only the consequences of the errors arising from the incomplete optimization along the easily distorted internal

(16) Petris, G. *Org. Mass. Spectrom.* **1990**, *25*, 83.

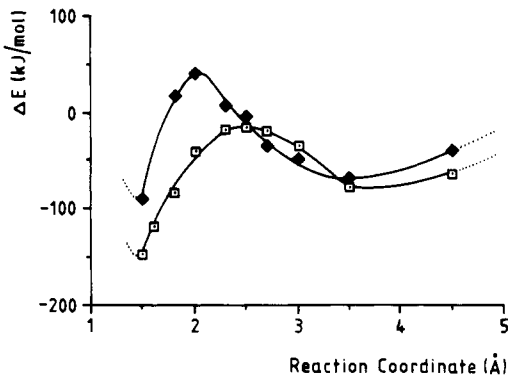

Figure 4. Energy profiles for reactions of benzene with the possible protonated methyl nitrate isomers: 1MN (⊡), mechanism 1; and 2MN (♦), mechanism 2.

coordinates. The calculated energies demonstrate that the barrier height (i.e., energy difference between the electrostatic complex and the TS) is about 45 kJ/mol lower in the case of reaction mechanism 1 than for the alternative mechanism 2.

The large size of the molecular systems and generally slow convergence of the geometry optimization did not allow computation of geometry parameters at higher than the Hartree–Fock level. However, the correlation energy contribution to the activation barrier height was evaluated at the MP4DQ level[17] (Table IV). There is no large difference between the HF and MP4DQ

(17) Because of the large number of geometrical parameters (57) and because some of them are characterized by flat potentials, the geometry of the complexes should be optimized on the level of calculation in order to get reliable results. However, it is assumed that the MP4DQ/3-21G and HF/3-21G structures are similar, at least, for the electrostatic complexes and the TS. It should also be noted that the MP4 calculation with a relatively small basis set (3-21G) probably underestimates the correlation energy. However, using a larger basis (including d-functions) should make these calculations very expensive, especially if further geometry optimization is necessary.

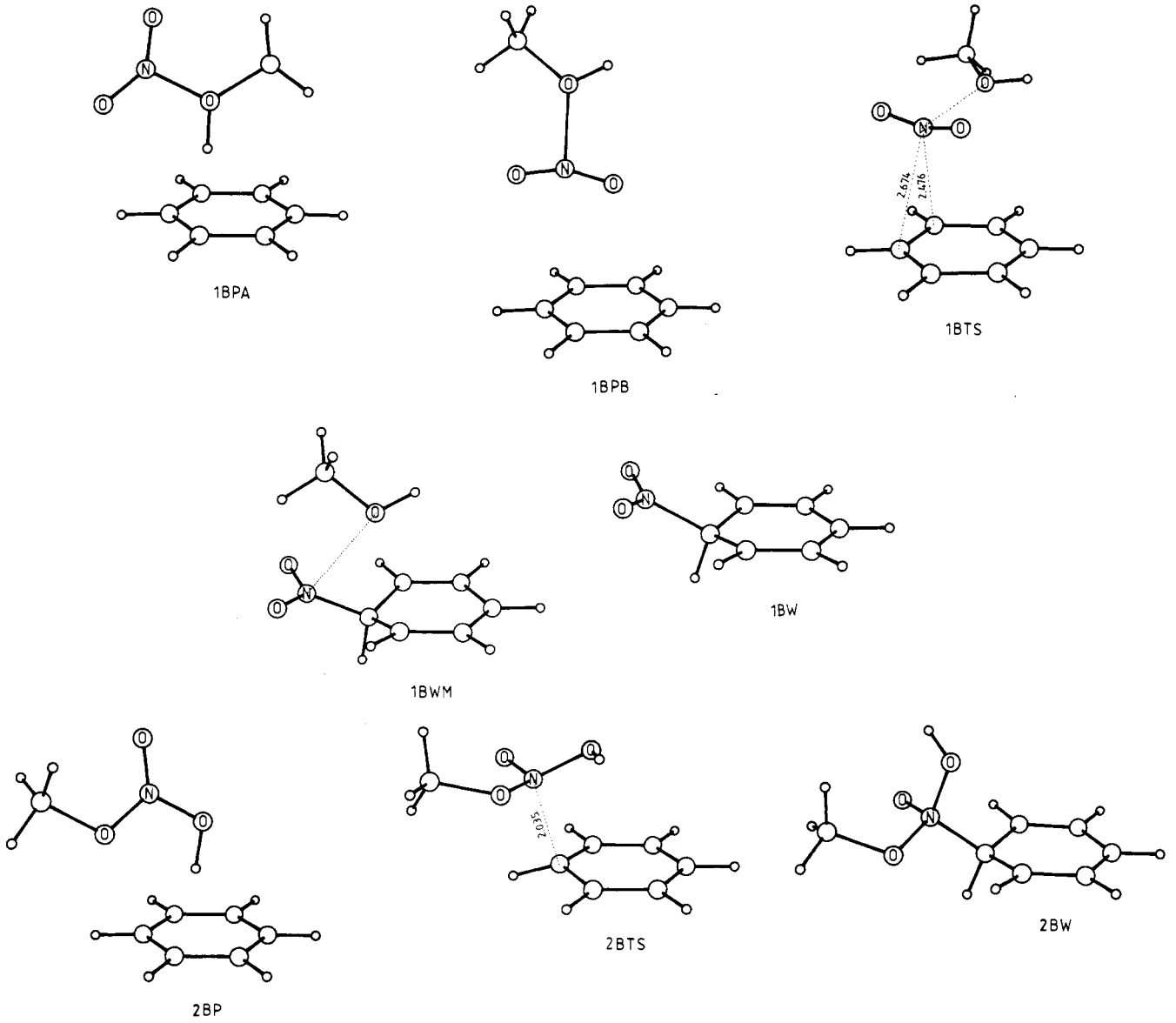

Figure 5. Stationary points calculated for the benzene nitration.

results with regard to the stability of electrostatic complexes, while HF overestimates the activation energy. Nevertheless, the difference in the barrier heights between the reaction paths is about 40 kJ/mol in favor of the classical reaction mechanism, close to 45 kJ/mol calculated from the HF data. This agreement in the results obtained at different computational levels can be due to the ionic nature of the interaction between the reactants in the electrostatic complexes and TS. Similarly to the HF results, the Wheland intermediate 1BWM is more stable than the covalent complex 2BW. However, their relative energies differ considerably on the HF and MP4 levels. Nevertheless, this discrepancy might arise from the lack of geometry optimization in the latter case.[18]

Structure of the Electrostatic Complexes. Both reagents form tight electrostatic complexes (1BPA, 1BPB, and 2BP) with the benzene (Figure 5). Their structures clearly show that the reagent is placed above, in the π-electron region of the benzene ring, in contrast to the Wheland intermediates, where the nitro group lies in the σ-plane. In π-complex 1BPA, even the methanol part of the reagent interacts with the benzene ring. Complexes 1BPA and 2BP are considerably more stable than the separated reactants, and their formation does not require any activation energy. The distance between the heavy atoms of the reactants is about 3–3.5 Å. Charge densities calculated from the Mulliken analysis show that there is practically no electron movement between the reactants: the total charge on the reagent 1MN is +0.911 e in 1BPA; on reagent 2MN the total charge is +0.931 e in 2BP.

Structure of the Transition States. The TS lies earlier on the reaction path of mechanism 1 (Figure 4), accompanied by the more stable product (σ-complex), than it does for the mechanism 2 case. Consequently, transition state structure 2BTS is more compact (RC = 2.035 Å) and has more σ-character than the earlier TS complex 1BTS. Comparing the geometry parameters of the benzene ring (Table V) in the transition state (1BTS) to

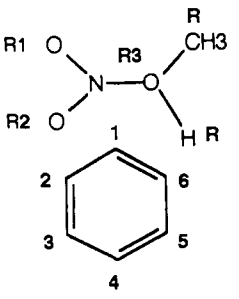

Figure 6. Notation of the atoms.

(18) The geometry of the benzene ring in the electrostatic complexes and TS is similar to that in the isolated substrate; however, it is markedly different in the Wheland intermediate (1BWM) or in the covalent complex (2BW); see Table V.

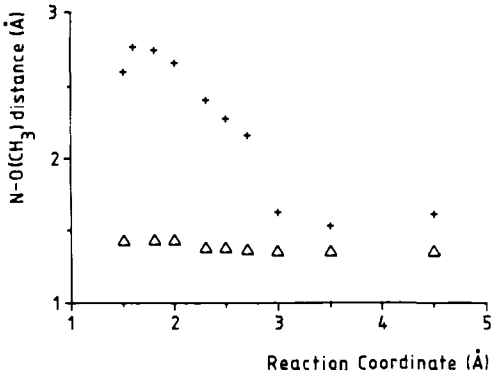

Figure 7. Dependence of the methanol–nitronium ion distance on the reaction coordinate for mechanism 1 (+) and mechanism 2 (Δ).

other stationary points of the reaction path, its similarity to the separated benzene ring (S1) or to the π-complex (1BPA) is obvious.

The two largest components of the transition vector (in internal coordinate representation) of 1BTS correspond to the reaction coordinate (C^1N bond) and the nitrogen–oxygen bond connecting the nitronium ion and methanol (NO^{R3} bond, in Figure 6). This implies that the reaction path 1 can be regarded as a desolvation process of the nitronium ion. It can also be illustrated by the dependence of the NO^{R3} distance on the length of the reaction coordinate (Figure 7, Table III). The distance between the nitronium ion and methanol is increased by 1.2 Å as the nitronium ion approaches the benzene ring. This emphasizes the vanishing influence of the methanol on the nitronium ion, especially on the TS ⇒ Wheland intermediate section of the reaction path. It is noteworthy that the NO^{R3} distance is practically independent of the RC value for mechanism 2 (Figure 7), indicating that methanol loss is prohibited.

If the interaction between the nitronium ion and its carrier is weak, a low activation barrier and early TS are expected. Thus the influence of the aromatic substrate on the barrier height should be weakened. This manifestation of the reactivity selectivity principle (RSP) might explain the decreased substrate selectivity of protonated fluoroalkyl nitrate compared to the protonated methyl nitrate reagent[5] (Table I).

The nitronium ion should be assigned to two carbon atoms in 1BTS, rather than to an individual one (Figure 5). Carbon–nitrogen distances are similar: 2.674 and 2.467 Å, respectively (see also Table V). Such bridged transition states have been reported for nitration of the dithienopyridinium ring[19] and for

Table V. Characteristic Geometrical Parameters for Stationary Points of Benzene Nitration[a]

b	1BPA	1BTS	1BW	S1[c]
C^1C^2	1.396	1.402	1.476	1.385
C^2C^3	1.395	1.383	1.356	1.385
C^3C^4	1.388	1.385	1.403	1.385
C^4C^5	1.386	1.396	1.412	1.385
C^5C^6	1.388	1.376	1.348	1.385
C^6C^1	1.384	1.395	1.479	1.385
C^1H^1	1.072	1.072	1.101	1.072
C^1N	3.535	2.476	1.492	–
C^2N	3.764	2.674	2.471	–
NO^{R1}	1.189	1.126	1.232	1.166
NO^{R2}	1.185	1.136	1.235	1.163
NO^{R3}	1.535	2.273	2.594	1.647
$O^{R3}C^{R}$	1.524	1.459	1.466	1.518
$O^{R3}H^{R}$	1.018	0.966	0.967	0.979
$C^1C^2C^3$	119.8	119.9	119.2	120.0
$C^2C^3C^4$	120.0	119.5	118.9	120.0
$C^3C^4C^5$	120.0	120.7	123.0	120.0
$C^4C^5C^6$	120.4	120.1	119.2	120.0
$C^5C^6C^1$	120.0	119.6	119.3	120.0
$C^6C^1C^2$	120.0	120.1	115.7	120.0
$C^6C^1H^1$	120.2	119.9	104.1	120.0
$C^2C^1H^1$	119.8	119.8	105.5	120.0
C^6C^1N	98.6	96.0	112.7	–
C^2C^1N	88.3	82.1	112.7	–
C^1NO^{R1}	136.5	104.1	116.2	–
C^1NO^{R2}	67.1	97.6	116.4	–
$O^{R1}NO^{R2}$	138.0	157.7	127.3	144.0
$NO^{R3}C^{R}$	119.1	126.5	96.6	124.6
$H^{R}O^{R3}C^{R}$	122.4	110.6	109.3	121.2

[a] Bond lengths in angstroms and angles in degrees. [b] See Figure 6 for notation of atoms. [c] Separated reactants of mechanism 1.

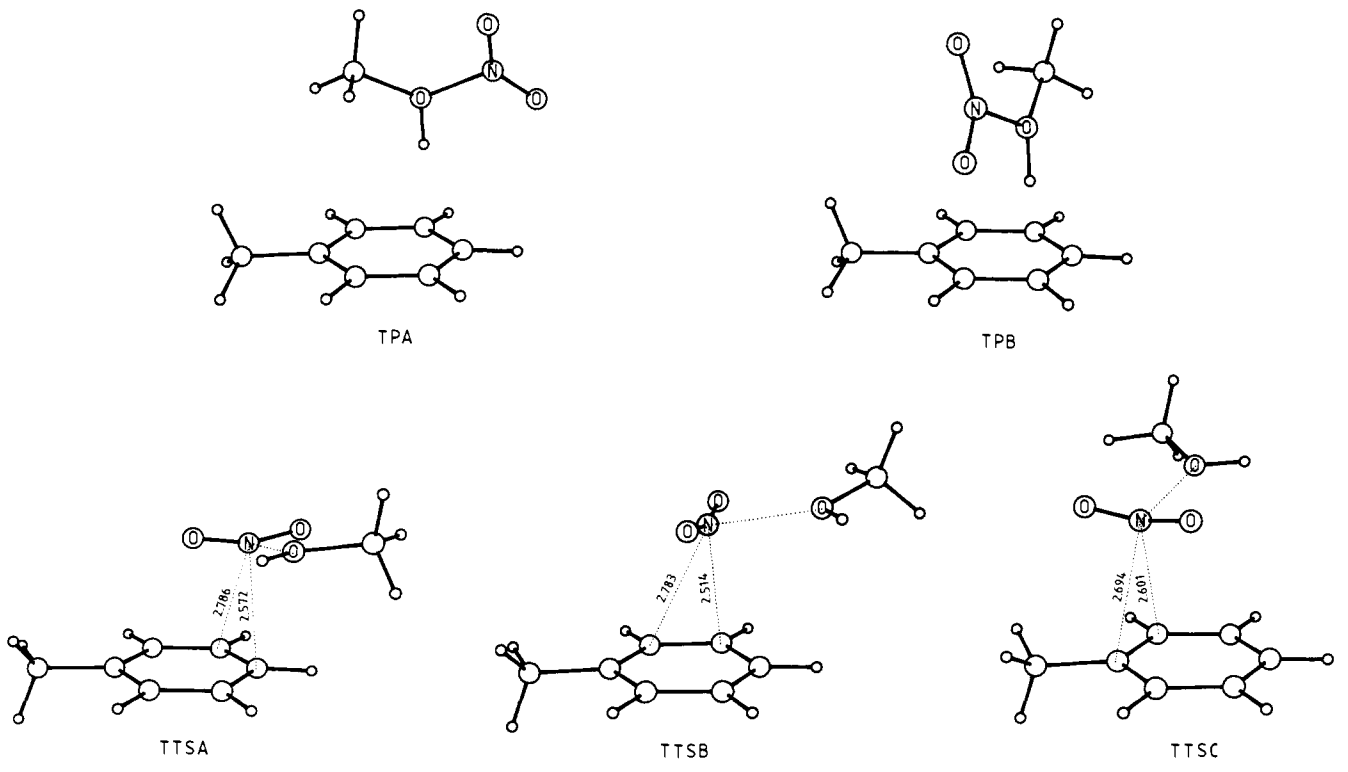

Figure 8. Stationary points calculated for the toluene nitration.

Table VI. Calculated Energies and Transition States of Toluene Nitration

species[a]	E_{total} (au)	ΔE (kJ/mol)	E_{rel}[b] (kJ/mol)
S[c]	−585.160 091	0.0	
TPA	−585.192 093	−84.0	0.0
TPB	−585.191 856	−83.4	0.6
TTSA	−585.170 515	−27.4	56.6
TTSB	−585.168 894	−23.1	60.9
TTSC	−585.170 811	−28.1	55.9

[a] See Figure 8 for notation. [b] Relative to the more stable π-complex. [c] Separated reactants.

certain olefin addition reactions.[20] The importance of a three-centered TS structure for substituted benzene derivatives is that the positional selectivity between the ortho and meta or meta and para positions would not be decided (or only partly) in the TS of the reaction.

Structure of Wheland Intermediates. It can be seen in Figure 5 that the nitronium ion is turned about 90° between the TS and WI in process 1. This implies that the methanol molecule, which is perpendicular to it, can be placed either above or under the nitro group of the Wheland intermediate. In the first case the geometry optimization of the WI–methanol complex (1BWM) can be forced to convergence, but the same problems appear as in the case of the optimization of the weakly bound complexes. In contrast, if the methanol is placed in a similar geometrical position, but *under* the nitro group, the optimization leads to spontaneous transfer of the "ipso" hydrogen atom to the methanol. This rapid formation of nitrobenzene makes process 1 irreversible and permits a short lifetime of the otherwise thermodynamically stable Wheland intermediate. The easy deprotonation of the Wheland intermediate is in accord with the experimental findings:[7,4] the lack of a deuterium isotope effect, and the fact that added bases (e.g., Et_3N) do not accelerate the reaction.

Nitration of Toluene. Two π-complexes were localized: TPA and TPB. In TPA the nitrating agent is in the symmetry plane perpendicular to the plane of the ring, while in TPB it is perpendicular to this plane (Figure 8). Despite the large difference in substrate–reagent orientation, the stability of these complexes is practically the same (Table VI). The stabilities of TPA and TBP are about 6 kJ/mol larger than for the π-complex in benzene nitration.

Three TS structures were obtained: TTSA, TTSB, and TTSC. The bridged structures are similar to that for benzene nitration (1BTS). The outcome of the reaction is not fully determined by the structure of the TS complexes. The conversion of TTSA can result in both para and meta nitrations, that of TTSB in meta and ortho nitrations, and that of TTSC in ortho and ipso nitrations. Their stabilities differ only by 1–5 kJ/mol. The barrier height is 5.4 kJ/mol lower than for the case of benzene nitration. The activation energy difference measured at 720 Torr of pressure using methane as bulk gas was 17.6 kJ/mol.[4] This discrepancy can certainly be due to the deficiencies of the theoretical model used and/or those matrix effects that we could not account for in this study. It is obvious that the substrate selectivity strongly depends[4,7] on the pressure and the applied bulk gas (Table I). Attinà and Cacace thoroughly discuss[4] the role of these factors in gas-phase nitration. The higher the pressure, the more effective is the thermolysis of the electrostatic complexes (π-complexes). A dense bulk gas (e.g., methane) can solvate the reactants, which further decreases the stability of the weakly bound complex. If the pressure was reduced or the methane (bulk gas) was exchanged for the less solvating hydrogen gas, the substrate selectivity was diminished (Table I), indicating a decreasing difference in activation energies. These conditions (i.e., low pressure and hydrogen as bulk gas) are similar to the matrix-isolated conditions (i.e., zero pressure and no solvating bulk gas at all) of the calculations presented herein. The matrix interactions certainly equalize the stability differences between the π-complexes. Assuming π-complexes of the same energy, and considering only the difference in TS complex stability, the barrier height is about 11 kJ/mol lower for toluene than for benzene nitration.

Table VII. Comparison of Wheland Intermediate Stabilities

species	E_{total} (au)	ΔE_i[a] (kJ/mol)
benzene	−229.419 446	
toluene	−268.240 210	
1BW	−431.968 714	0.0
toluene–NO_2^+		
ortho	−470.800 502	−29.0
meta	−470.794 976	−14.5
para	−470.806 586	−44.9

[a] Isodesmic energy. Defined by the following equation: $\Delta E_i = E_{benzene} - E_{toluene} + E_{toluene\text{–}NO_2^+} - E_{benzene\text{–}NO_2^+}$.

The relative stability of Wheland intermediates (Table VII) correlates well the substrate and positional selectivity (Table I). However, it should be pointed out that the relative positional selectivities predicted by the stability differences of the Wheland intermediate complexes are strongly overestimated. It has been demonstrated[21] that the Wheland intermediate stabilities can be correlated very well with the σ^+ substituent constants, but the reaction constant, ρ, is 2 and 5 times larger than the experimentally found condensed-phase and gas-phase values,[7] respectively. However, the question is then, how positional selectivity is determined in the aromatic nitration reaction.

The bridged TS is inevitably followed by a bifurcation point on the reaction path. Reaction trajectories, starting at this bifurcation point, lead to the corresponding Wheland intermediates. As the decomposition (deprotonation) of the Wheland intermediate is a fast and irreversible process, the steepness of the potential energy surface at the bifurcation point should define the positional selectivity between the carbon atoms assigned to the corresponding TS. Consequently, the quantitative isomer distribution is not predictable from the energy difference of the Wheland intermediates. However, the slopes of the reaction trajectories are certainly proportional to the stability of the Wheland intermediates. This implies that at least the qualitative (or semiquantitative) reactivity order can be anticipated by the Wheland intermediate stabilities.

An illustration of this theory can be the analysis of the electrostatic maps calculated in planes parallel to that of the toluene molecule. Electrostatic maps calculated at 2–3.5 Å from the toluene plane (Figure 9a–c) do not reflect the individual nuclear positions at all. In contrast, at distances getting closer to the ring plane the variation in energy becomes larger and larger (Figure 9d–f). Finally a distance is reached at which well-defined sections isolate the electrostatic potential of the individual nuclear positions (Figure 9g). It can be assumed that the bifurcation point of the hypothetical reaction trajectories for the positive point charge–toluene interaction should be somewhere between 1.5 and 1.3 Å. The evolution of a bifurcation point of the nitration reaction can be conceived in a similar way.

Extension to Condensed Phase. Since the gas-phase reaction between protonated methyl nitrate and aromatic substrates can be considered to be an electrophilic aromatic nitration reaction by a methanol-solvated nitronium ion, it is assumed that some of the suggestions from the present theoretical study can be extended to the condensed-phase reactions.

1. In the course of the nitration reaction the nitronium ion should overcome a desolvation barrier (DSB). The barrier height depends on the strength of the interaction between the nitronium ion and the matrix. The matrix can be a carrier (e.g., methanol as in this case or acetate ion as in the case of nitration by acetyl

(19) Szabó, K. J.; Hörnfeldt, A.-B.; Gronowitz, S. *THEOCHEM*, in press.
(20) Wünsch, E.; Sodupe, M.; Lluch, J. M.; Olivia, A.; Bertran, J. *THEOCHEM* **1988**, *170*, 225. Minato, T.; Inagaki, S. *J. Chem. Soc., Chem. Commun.* **1988**, 532. Hommes, N. J. R. v. E.; Schleyer, P. v. R. *J. Org. Chem.* **1991**, *56*, 4074.

(21) Szabó, K. J. *THEOCHEM* **1988**, *181*, 1.

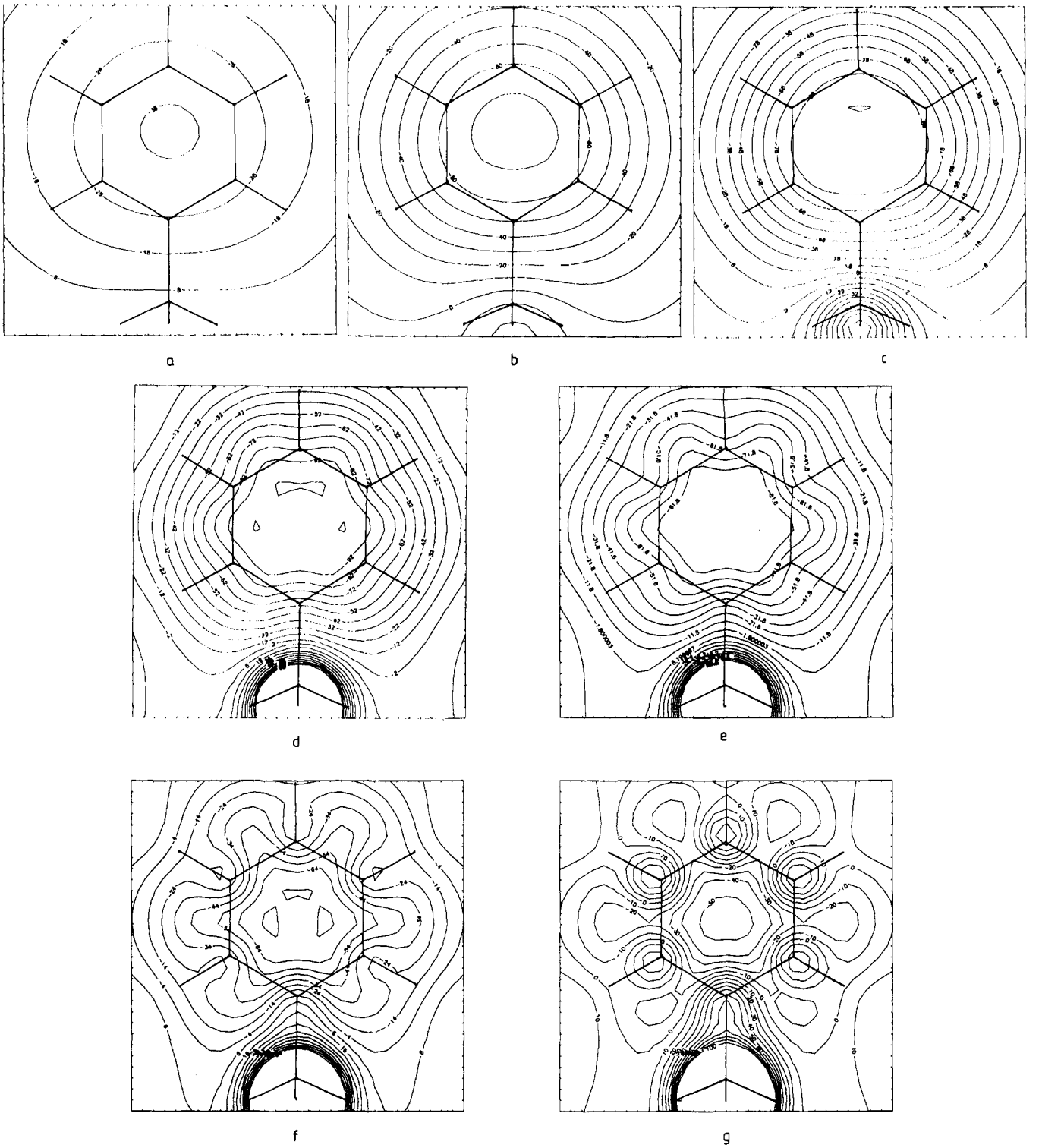

Figure 9. Electrostatic potentials in planes parallel with the ring plane of toluene. Distances from the ring plane are as follows: (a) 3.5 Å; (b) 2.5 Å; (c) 2.0 Å; (d) 1.5 Å; (e) 1.4 Å; (f) 1.3 Å; (g) 1.2 Å. Energy levels are given in kJ/mol.

nitrate), counterion (e.g., nitration by NO_2BF_4), complexing agent (e.g., nitration by NO_2BF_4–crown ether complex), or even the solvent shell. If the interaction between the matrix and nitronium ion is strong, higher substrate selectivity is expected. (See the discussion on substrate selectivity when a fluoroalkanol is used as carrier.)

2. The final positional selectivity develops independently of the desolvation barrier. It is assumed to be determined by bifurcation points related to the corresponding TS and Wheland intermediate on the potential energy surface. As this point is placed in the TS ⇒ WI section of the reaction path, after the loss of matrix, it is conceivable that its evolution is only slightly influenced by matrix effects.

Finally, the limitations of this theory should be indicated. If the substrate is considerably less reactive or the matrix–nitronium ion interaction is much stronger than in the examples given here, a later TS is expected than found for the benzene or toluene nitration. Repulsion between the positively charged reactants should be responsible for the intrinsic barrier (IB) in the nitration of protonated heteroaromatics.[12,13,19] This implies that the matrix effects are expected to play a completely different role than in the case of the DSB-type process of uncharged aromatic substrates.

Acknowledgment. We thank the NSC (National Superda-

torcentrum vid Universitet i Linköping) for generous grants of computer time on the Cray X-MP/416 supercomputer. Grants from the Swedish Natural Science Research Council to S.G. are gratefully acknowledged.

Registry No. Benzene, 71-43-2; nitronium, 14522-82-8; methyl nitrate (protonated), 99573-80-5; toluene, 108-88-3.

Supplementary Material Available: Tables giving internal coordinate systems (in Z-matrix form) and optimized geometrical parameters (36 pages). Ordering information is given on any current masthead page.

The Puckering Inversion Barrier and Vibrational Spectrum of Cyclopentene. A Scaled Quantum Mechanical Force Field Algorithm

Wesley D. Allen,*,† Attila G. Császár,‡ and David A. Horner§

Contribution from the Department of Chemistry, Stanford University, Stanford, California 94305, Failure Analysis Associates, Inc., 149 Commonwealth Drive, Menlo Park, California 94025, and Departments of Chemistry and Physics, North Central College, Naperville, Illinois 60566.
Received February 3, 1992

Abstract: High-level ab initio quantum chemical studies have been performed to ascertain the equilibrium molecular structure and ring-puckering inversion barrier of cyclopentene, as well as the complete infrared and Raman spectra of cyclopentene-d_0, -*1*-d_1, -*1,2,3,3*-d_4, and -d_8. The planar (C_{2v}) and puckered (C_s) structures of cyclopentene have been optimized at the DZ(d) SCF and MP2 levels, and reasonable agreement with available experimental data is found. The DZ(d) MP2 prediction for the puckering angle is 23.4°, which compares favorably with several experimental values in the range 22–26°. High-level electron correlation treatments with extended basis sets are found to be necessary to converge the predicted puckering inversion barrier. In accord with experimental values, a final theoretical proposal of 235 ± 20 cm^{-1} is derived for the vibrationless inversion barrier from a combination of TZ(d,p) MP4 and PZ(3d2f,2p1d) MP2 results. The fundamental vibrational frequencies (including intensity and polarization data) of cyclopentene isotopomers have been obtained from DZ(d) SCF force constants by using the scaled quantum mechanical (SQM) force field procedure. An improved SQM algorithm has been formulated which allows facile optimization of empirical scale factors to determine optimal quadratic force fields. Numerous reassignments are proposed among the 128 observed fundamental frequencies of the four isotopomers considered. It is shown that zero-point vibrational effects engender a substantial contribution to the empirically derived puckering inversion barrier.

Introduction

As discussed in a 1979 review by Carreira, Lord, and Malloy,[1] many of the fundamental issues pertaining to low-frequency vibrations in small ring compounds are encountered in the investigation of representative molecules such as cyclobutane, cyclopentene, trimethylene oxide, 1,4-dioxadiene, tetrahydrofuran, and 1,4-dioxene. In this sense the cyclopentene molecule constitutes a prototype of large-amplitude, ring-puckering motion in the gas phase. In general, the low-frequency vibrational spectra of such molecules can be interpreted satisfactorily via one- and two-dimensional quantum mechanical models for ring puckering and/or twisting; however, coupling with the zero-point vibrational motions of the high-frequency normal modes must be considered in the analysis. In many cases the low-frequency spectroscopic information obtainable in the far-infrared region is incomplete, and the ring-puckering vibrations must be characterized from resulting difference bands associated with reference fundamentals in the mid-infrared region. Therefore, to fully resolve questions pertaining to the puckering dynamics of a small ring compound such as cyclopentene, not only are reliable results required for the equilibrium configuration and the ring puckering potential function but also a definitive analysis of the complete vibrational spectrum is needed.

Due to its prototypical characteristics, cyclopentene has become one of the most thoroughly studied examples of pseudo-four-membered-ring molecules with a double-minimum potential function for low-frequency puckering vibrations.[1-4] Over the course of the last few decades, the far-infrared,[9,14,15,20] mid-infrared,[5-8,12,13,16-21] Raman,[10-15,18-22] and microwave[23-25] spectra

† Stanford University.
‡ Stanford University; Failure Analysis Associates, Inc.
§ North Central College.

(1) Carreira, L. A.; Lord, R. C.; Malloy, T. B. *Top. Curr. Chem.* **1979**, *82*, 1.
(2) Laane, J. *Pure Appl. Chem.* **1987**, *59*, 1307.
(3) Harthcock, M. A.; Laane, J. *J. Mol. Spectrosc.* **1982**, *91*, 300.
(4) Malloy, T. B., Jr.; Bauman, L. E.; Carreira, L. A. *Top. Stereochem.* **1979**, *11*, 97.
(5) Beckett, C. W.; Freeman, N. K.; Pitzer, K. S. *J. Am. Chem. Soc.* **1948**, *70*, 4227.
(6) Sverdlov, L. M.; Krainov, E. N. *Opt. Spectrosc. (USSR)* **1959**, *6*, 214.
(7) LeRoy, A.; Thonvenout, J. C. *C. R. Acad. Sci.* **1967**, *B37*, 545.
(8) Ueda, T.; Shimanouchi, T. *J. Chem. Phys.* **1967**, *47*, 5018.
(9) Laane, J.; Lord, R. C. *J. Chem. Phys.* **1967**, *47*, 4941.
(10) Durig, J. R.; Carreira, L. A. *J. Chem. Phys.* **1972**, *56*, 4966.
(11) Chao, T. H.; Laane, J. *Chem. Phys. Lett.* **1972**, *14*, 595.
(12) Wertz, D. W.; Bocian, D. F.; Hazouri, M. J. *Spectrochim. Acta* **1973**, *29A*, 1439.
(13) Harris, W. C.; Longshore, C. T. *J. Mol. Struct.* **1973**, *16*, 187.
(14) Villarreal, J. R.; Bauman, L. E.; Laane, J.; Harris, W. C.; Bush, S. F. *J. Chem. Phys.* **1975**, *63*, 3727.
(15) Villarreal, J. R.; Bauman, L. E.; Laane, J. *J. Phys. Chem.* **1976**, *80*, 1172.
(16) Villarreal, J. R.; Laane, J.; Bush, S. F.; Harris, W. C. *Spectrochim. Acta* **1979**, *35A*, 331.
(17) Green, W. H. *J. Chem. Phys.* **1970**, *52*, 2156.
(18) Besnard, M.; Lassegues, J.-C.; Guissani, Y.; Leicknam, J.-L. *Mol. Phys.* **1984**, *53*, 1145.
(19) Villarreal, J. R. Ph.D. Thesis, Department of Chemistry, Texas A&M University, 1976.
(20) Lascombe, J.; Cavagnat, D.; Lassegues, J. C.; Rafilipomanana, C.; Biran, C. *J. Mol. Struct.* **1984**, *113*, 179.
(21) Rafilipomanana, C.; Cavagnat, D.; Lassegues, J. C. *J. Mol. Struct.* **1985**, *129*, 215.
(22) Rafilipomanana, C.; Cavagnat, D.; Cavagnat, R.; Lassegues, J. C.; Birat, C. *J. Mol. Struct.* **1985**, *127*, 283.

0002-7863/92/1514-6834$03.00/0